Computers and Concrete, Vol. 4, No. 1 (2007) 49-66
DOI: http://dx.doi.org/10.12989/cac.2007.4.1.049

Validation of 3D crack propagation in plain concrete. Part I: Experimental investigation - the PCT3D test

C. Feist and G. Hofstetter†

University of Innsbruck, Faculty of Civil Engineering, Technikerstrasse 13, A-6020 Innsbruck, Austria
(Received April 30, 2006, Accepted February 5, 2007)

Abstract. The objective of this paper is to provide experimental data on the propagation of curved crack-surfaces and the respective load-displacement diagrams for the validation of numerical models for cracking of concrete, subjected to three-dimensional stress states. To this end beam-shaped specimens are subjected to combined bending and torsional loading, leading to the formation of a spatially curved crack-surface. The experimental data contain the evolution of the load and of the strains at selected points in terms of the crack mouth opening displacement and the propagation of the crack surface.

Keywords: finite element method; concrete cracking.

1. Introduction

In recent years considerable emphasis has been put on the development of models for the numerical simulation of cracking of plain concrete subjected to three-dimensional stress states. In addition to the classical smeared crack approach for 3D fracture problems (cf., e.g. Jefferson, *et al.* 2004), the strong discontinuity approach has gained wide popularity for numerical simulations of concrete fracture. It results in finite elements which are enhanced either by an elemental enrichment or a nodal enrichment of the interpolation functions in order to represent the displacement discontinuity at a crack. The former method is known as elements with embedded discontinuities whereas the latter approach is denoted as Partition of Unity Finite Element Method (PUFEM) or Extended Finite Element Method (XFEM). Since this paper is devoted to experimental work, only a few papers are cited as representatives for the large body of literature (Sukumar, *et al.* 2000, Jirásek, 2000, Oliver, *et al*. 2003, Gasser, *et al*. 2005).

However, for the validation of 3D fracture models for cracking of plain concrete only results from a very limited number of well documented 3D fracture tests is available. The often used anchor pull out tests are characterized by axial symmetry. One of the rare examples of 3D tests are torsional tests (e.g., Brokenshire 1996, Jefferson and Bennett 2005). Hence, it is the objective of this paper to provide further experimental data for the validation of such models, containing the development of curved crack-surfaces and the respective load-displacement diagrams as well as relations between the strains at selected points and the applied load. To this end beam-shaped specimens of 600 mm length, 500 mm span with a square shaped cross-section of 180×180 mm are designed. Five identical specimens are subjected to a three-dimensional stress state resulting from combined bending and torsional loading and leading to the formation of a spatially curved crack-surface.

† Corresponding Author, E-mail: Guenter.Hofstetter@uibk.ac.at

2. Experiments

2.1. Specimens

The specimens are beams of 600 mm length, with a quadratic cross section of 180×180 mm (Fig. 1). The span (distance between the supports) is chosen as 500 mm. The axes of the supports are located at an offset of 50 mm from the respective end of the beam and the tensile face. The supports consist of steel bars with 30 mm diameter and steel sleeves embedded in the concrete beam (Fig. 1, detail a).

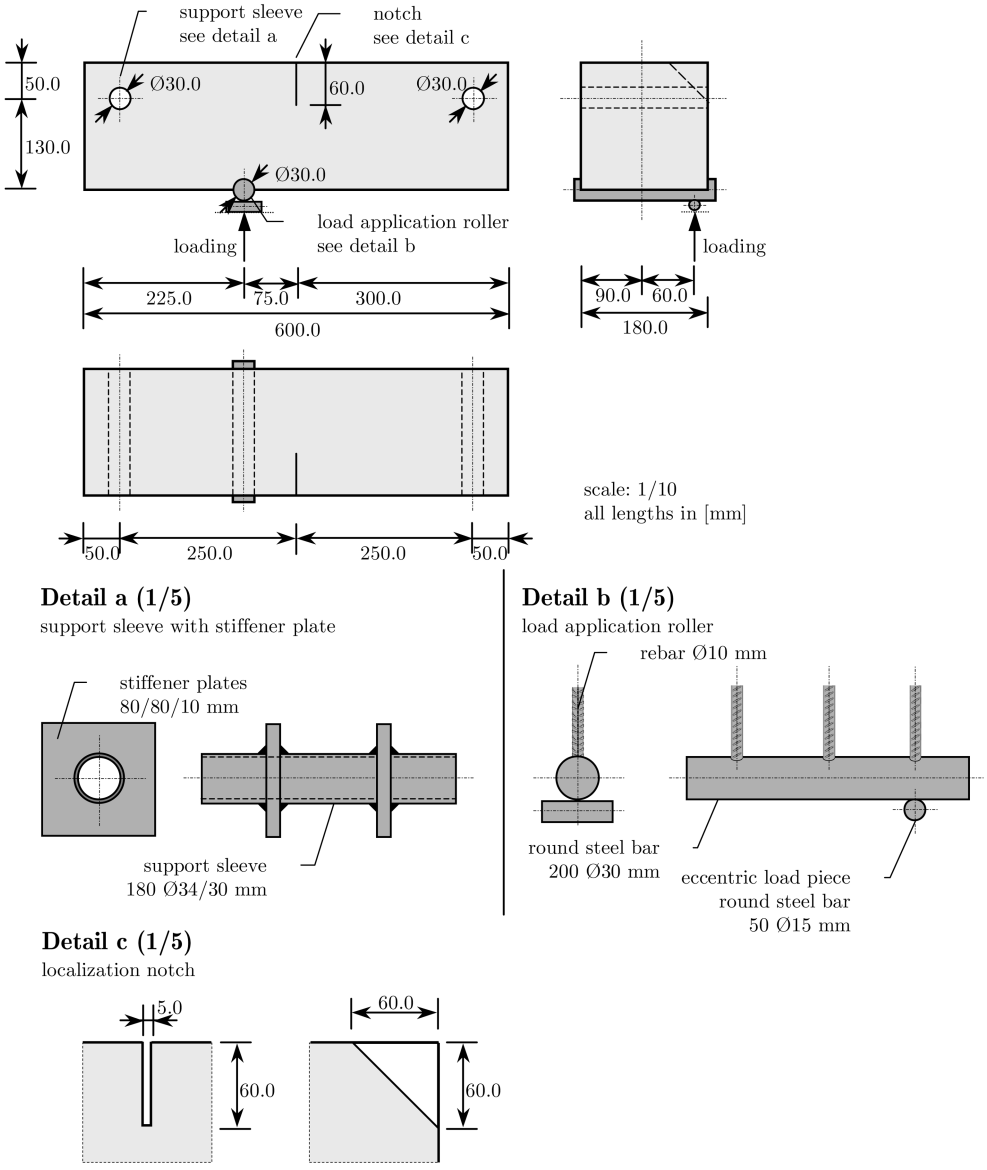

Fig. 1 Test specimen

Additional stiffener plates are welded onto the steel sleeves to provide an optimal load distribution and to prevent crushing of the concrete in these areas. The load is applied by means of a load application roller consisting of a steel bar of 30 mm diameter (Fig. 1, detail b). Three short pieces of reinforcement bars are welded onto the roller to provide a good compound between the roller and the concrete.

To stress the specimen by bending and by torsion simultaneously, an eccentric load is applied by using a steel bar of 15 mm diameter and 50 mm length, which is placed in longitudinal direction below the load application roller at a distance of 60 mm with respect to the beam axis. Hence, the transverse load application roller serves as a means to distribute the point load and to prevent extensive crushing in the vicinity of the point of load application (Fig. 1, detail b). A notch with an isosceles triangular shape of 60 mm leg length is provided at mid-span (Fig. 1, detail c). It serves as the location of crack initiation from which the crack surface propagates along the upper and lateral faces independently, approaching the beam section at the point of load application.

For all specimens formworks of laminated boards of 20 mm thickness with a smooth surface are employed. The support sleeves with the stiffener plates and the load application roller are mounted together with the formwork before concreting. Special attention is put on the precision of the formwork. It is especially crucial to keep precise measures of the positions of the support sleeves: The formwork is designed to cast the specimens from the lower face (the face containing the load application roller). This guarantees a constant concrete quality with respect to the width of the specimen. Additionally, this provides smooth lateral faces allowing for good observation of crack propagation during the experiment. A table-vibrator is used to compact the specimens. All specimens are stored in water during the first seven days after concreting and kept on air for the remainder of the hardening period of 28 days. One day after concreting the mould is removed from the specimens. The notches of the specimens are cut by a circular saw at the end of the hardening period.

2.2. Test setup

All experiments are carried out with a universal hydraulic load frame of type Instron 8802 (Instron 2002). This frame allows for a cylinder lift height of ±125 mm and test loads up to 100 kN. To allow for a proper support of the particular specimens a special support frame is constructed. It consists of a base plate, four support columns and support blocks. It is designed to be mounted on the base of the hydraulic load frame and to be adjusted to the required eccentric position of the specimen. Each of the four support blocks is equipped with one elongated hole carrying the support roller of the specimen. The load is applied by the load cylinder acting on a constraint-free coupling device with two hinges. This device transmits the force onto the support frame surrounding the specimen, from which the test load is applied onto the load application roller of the specimen as a point-load.

The installation of the specimens requires the support frame to be fastened with an eccentricity of 60 mm (in transverse direction) and 75 mm (in longitudinal direction), respectively. The overall test setup is depicted in Fig. 2.

2.3. Instrumentation

The vertical displacement at the point of load application is measured by an inductive

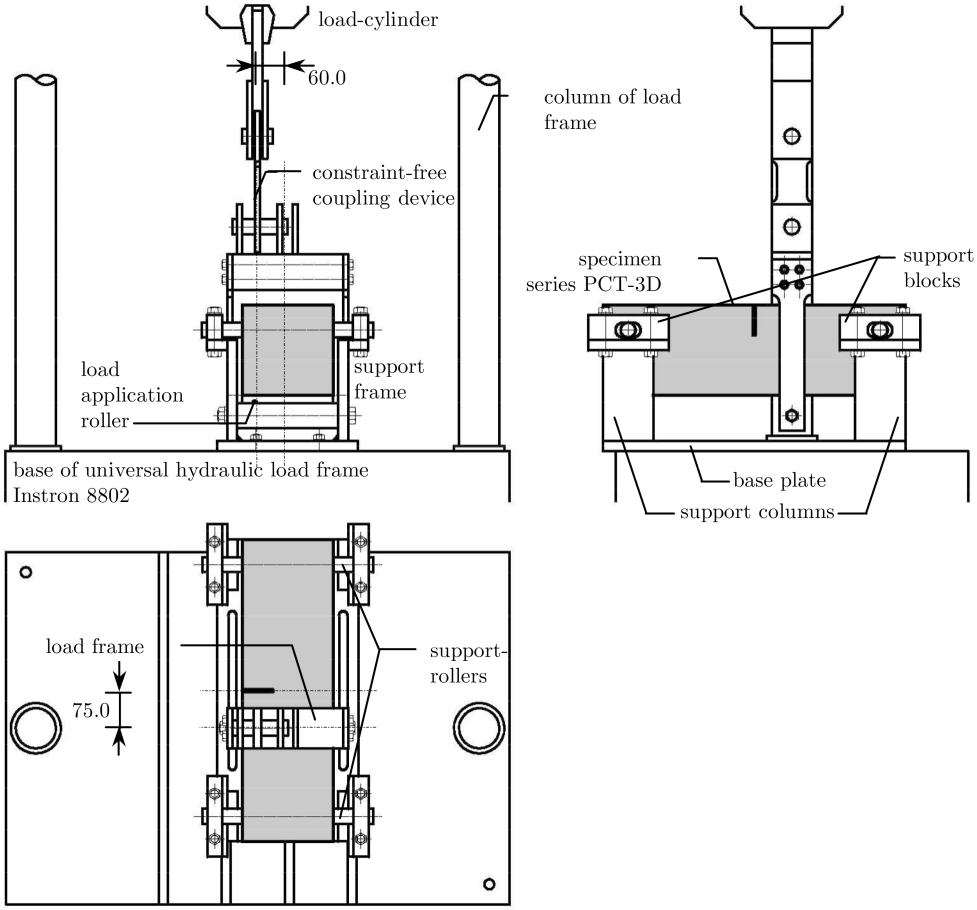

Fig. 2 Test setup

Table 1 Instruments

Instrument	Manufacturer	Type	Accuracy
load frame	Instron	8802	$\times 10^{-2}$ mm ±10 N
IDT	Hottinger Baldwin	WTK ±10 mm	$\pm 10^{-3}$ mm
SG	Hottinger Baldwin	10/120 LY61	±1 μm/m
EXT	Instron	2620/601	$\pm 10^{-3}$ mm

displacement transducer (*IDT*). It is denoted as *IDT2* in Fig. 3. To compensate the displacements from the support frame two additional IDTs are installed at the support rollers, denoted as *IDT* 1 and *IDT* 4 in Fig. 3. One additional IDT (i.e. *IDT* 3) is installed at the tensile face of the specimens in the longitudinal symmetry plane at a distance of 175 mm and 325 mm, respectively, from the supports.

Strain gauges (SG) are located on the lateral faces and on the top (i.e. tensile) face. SG 1 is located on the top face at midspan of the specimen. SG 2 is found on the top face at the edge opposite to the notch. SG 3 and SG 5 are located at mid-span and mid-height on the front and rear

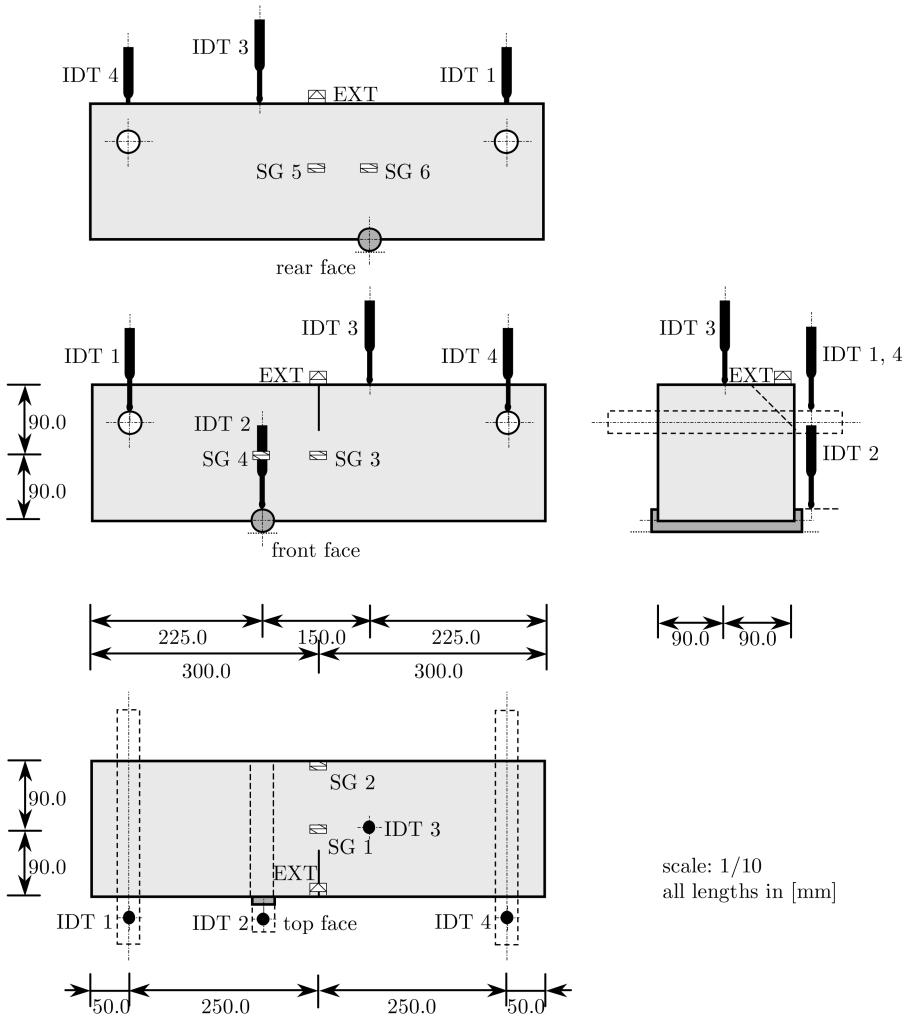

Fig. 3 Instrumentation

face, respectively. SG 4 and SG 6 are placed at the same height as SG 3 and SG 5 at the same longitudinal position as the load application roller. An extensometer EXT is located across the notch at the front edge of the top-face. The used types of instruments are summarized in Table 1.

2.4. Realization of the experiments

The experiments are carried out by prescribing a constant rate of displacement of the load cell of 2.0×10^{-2} mm/min until a load of 20.0 kN is attained. Up to this load level the specimens are in the regime of elastic material behavior. Then a constant rate of crack mouth opening displacement of 8.0×10^{-4} mm/min is prescribed.

During the experiments the data from all instruments are recorded. Two data amplifiers of type *Spider8* (Instron 2002) are used for the measurement acquisition. The data is transmitted to a PC equipped with the data storage software *Dia/Dago* (Instron 2002).

3. Material properties

The tests for the determination of material parameters and the employed samples are listed in Table 2. All tests are conducted in accordance to ENV-2006, 1990 and CEB-FIP (1991), respectively. The samples are compacted and stored in the same manner as the test specimens.

3.1. Concrete mix

The five identical test specimens are made of plain concrete. The maximum aggregate size is chosen as 8 mm, which provides a good workability for the relatively small specimens. A Portland cement of quality PZ 275 is employed. The water/cement-ratio is 0.55 providing a consistency index of K3 to ensure a good concrete-workability. No admixtures are used. The concrete mix design can be seen from Table 3. The mean value of the density is determined from the cubic samples as $\rho = 2449$ kg/m^3.

3.2. Uniaxial compressive strength

The mean value of the uniaxial compressive strength is determined from the three cubic samples. Since the uniaxial compressive strength according to ENV-2006 (1990) refers to the compressive strength of cylindrical samples, the latter is computed from the approximate relation as

Table 2 Samples used for the determination of material parameters

Material property		Shape of sample	Dimensions [mm]	Number
Uniaxial compressive strength	f_c	cube	150/150/150	3
Density[a]	ρ			
Uniaxial tensile strength	f_{ct}	prism	160/40/40	3
Young's modulus[b]	E			
Poisson's ratio[b]	ν			
Fexural tensile strength	$f_{ct,fl}$	prism	160/40/40	3
Splitting tensile strength	$f_{ct,sp}$	cylinder	∅ 150/300	3
Specific fracture energy	G_f	prism	160/40/40	5

[a]measured on the same samples as f_c
[b]measured together with f_{ct}

Table 3 Concrete mix design

Aggregate (grain size 0-1 mm):	681.13 kg/m^3
Aggregate (grain size 1-4 mm):	973.05 kg/m^3
Aggregate (grain size 4-8 mm):	291.91 kg/m^3
Portland cement PZ 275:	320.00 kg/m^3
Water:	176.00 kg/m^3

Table 4 Compressive strength, determined from cubic samples

Sample #	$f_{c,cube}$ [N/mm^2]
1	51.78
2	49.56
3	51.78
$\mu = f_{cm,cube}$	51.04
$\lvert\sigma\rvert$	1.05

Table 5 Young's modulus, Poisson's ratio and uniaxial tensile strength

Sample #	E_c [N/mm^2]	ν [–]	f_{ct} [N/mm^2]
1	34684.30	0.1753	4.73
2	39708.00	0.1928	4.86
3	37485.50	0.2101	4.91
μ	37292.60	0.1927	4.83
$\|\sigma\|$	2055.45	0.014	0.37

$$f_{c,cyl} = 0.786 \cdot f_{c,cube} \,. \tag{1}$$

The compressive strengths determined from the three samples are shown in Table 4 along with the mean value μ and the standard deviation $|\sigma|$. From Eq. (1) $f_{c,cyl}$ is obtained as 40.12 N/mm^2.

3.3. Tensile strength and elastic properties

For the determination of the uniaxial tensile strength f_{ct}, the Young's modulus E_c and the Poisson's ratio ν the prismatic samples are used. All three aforementioned properties are determined within the same test. The uniaxial tensile strength is obtained from the failure load of a sample. The Young's modulus is determined by averaging values from two strain gauges applied in longitudinal direction, whereas the Poisson's ratio is found by averaging values from two strain gauges in transverse direction. All strain gauges are attached to the two opposite lateral faces of the prisms.

The experimentally obtained value for the Young's modulus, the Poisson's ratio and the uniaxial tensile strengths for the three samples and the corresponding mean values and standard deviations are listed in Table 5.

Although the uniaxial tensile strength of concrete is the adequate property to describe tensile failure, it is difficult to be determined as it is commonly characterized by relatively large scatter of the experimentally determined values. Thus, the tensile strength is often estimated from the characteristic compressive strength f_{ck} (CEB-FIP 1991) by

$$f_{ctm} = f_{ctko,m} \left(\frac{f_{ck}}{f_{cko}} \right)^{2/3} \tag{2}$$

with f_{ck}=f_{cm}–8 N/mm^2 as the characteristic value (5% fractile value) of the compressive strength and f_{cko}=10 N/mm^2 and $f_{ctko,m}$=1.40 N/mm^2 as proposed by CEB-FIP (1991). The lower and upper bounds for the characteristic tensile strength $f_{ctk,\min}$ and $f_{ctk,\max}$ may be estimated by

$$f_{ctk,\min} = f_{ctko,\min} \left(\frac{f_{ck}}{f_{cko}} \right)^{2/3}, \quad f_{ctk,\max} = f_{ctko,\max} \left(\frac{f_{ck}}{f_{cko}} \right)^{2/3} \tag{3}$$

with $f_{ctko,\min}$=0.95 N/mm^2 and $f_{ctko,\max}$=1.85 N/mm^2.

In König and Grimm (1996) and FIP (1999) an estimate for the tensile strength from the material's mean compressive strength f_{cm} is proposed by

$$f_{ctm} = f_{ctmo} \cdot \ln \left(\frac{f_{cm}}{f_{cmo}} \right) \tag{4}$$

Table 6 Estimates of the tensile strength, determined from the characteristic compressive strength f_{ck}, the mean value of the cylindrical compressive strength $f_{c,cyl}$, the splitting tensile strength $f_{ct,sp}$ and the flexural tensile strength $f_{ct,fl}$ as well as lower and upper bounds for the tensile strength

f_{ctm} [N/mm^2]	Estimate of f_{ctm} from				Bounds	
	f_{ck}	$f_{c,cyl}$	$f_{ct,sp}$	$f_{ct,fl}$	$f_{ctk,min}$	$f_{ctk,max}$
4.83	3.05	3.42	3.20	4.02	2.07	4.03

with f_{ctmo}=2.12 N/mm^2 and f_{cmo}=10 N/mm^2.

It is noted that the mean value of the experimentally determined numerical tensile strength of f_{ctm} =4.83 N/mm^2 is larger than the respective estimates and even exceeds the upper bound of the tensile strength of 4.03 N/mm^2.

In addition to the uniaxial tensile strength also the flexural tensile strength $f_{ct,fl}$ and the splitting tensile strength $f_{ct,fl}$ are determined. The first is obtained by means of the prismatic samples like the ones used for determination of the uniaxial tensile strength, which are subjected to a symmetric three-point bending test. The splitting tensile strength is found by loading cylindrical specimens of 150 mm diameter and 300 mm height. The values of the flexural tensile strength $f_{ct,fl}$ and the splitting tensile strength $f_{ct,sp}$ are compared with the uniaxial tensile strength according to the relations proposed by CEB-FIP (1991) and FIP (1999) as

$$f_{ctm} = 0.90 \cdot f_{ct,sp}, \quad f_{ctm} = f_{ct,fl} \frac{\alpha_{fl}(h_b/h_o)^{0.7}}{1+\alpha_{fl}(h_b/h_o)^{0.7}} \tag{5}$$

where h_b is the depth of the prismatic specimen and h_o=100 mm. In CEB-FIP (1991) a value α_{fl}=1.5 is proposed. The second relation given in Eq. (5) is valid for h_b > 50 mm according to CEB-FIP (1991), which is not fullfilled by the available samples. Nevertheless, the results of the proposed relation are also used as estimates of the uniaxial tensile strength.

The estimates of the tensile strength obtained from Eqs. (2), (4) and (5) as well as the upper and lower bounds of the tensile strength from Eq. (3) are summarized in Table 6.

3.4. Specific fracture energy

Following the recommendations RILEM (1985) three-point bending tests are used for determining the specific fracture energy. For a maximum aggregate size of 8 mm beams of 100 mm depth and width, 840 mm length and 800 mm span are recommended. Samples of this size were not available, as it was initially planned to determine the specific fracture energy by direct tension tests on the prismatic samples with dimensions of 160×40×40 mm. Hence, the latter are employed for the three-point bending tests. According to Hillerborg (1985) the depth and width of the fracture area should be at least three times the maximum aggregate size. Hence, a notch of 10 mm depth and a width of approximately 3 mm over its entire height is sawn under wet conditions, resulting in a fracture area of 30×40 mm. The tests are driven in a displacement controlled fashion. One single extensometer is applied at the notch to measure the crack mouth opening displacement.

The specific fracture energy G_f is determined by integration of the curve representing the relationship between the load and the crack mouth opening displacement instead of integrating the load-deflection curve as proposed by RILEM (1985). The values of these integrals are then divided

Table 7 Values of the specific fracture energy

Sample #	G_f [Nmm/mm^2]
1	0.0691
2	0.0741
3	0.0793
4	0.0664
5	0.0863
μ	0.0750
$\|\sigma\|$	0.0072
Estimate	0.0660

by the fracture or ligament area (i.e. the net cross-section of the beams) according to RILEM (1985). The proposed method yields reliable and well comparable results for the different samples. The values for the specific fracture energy G_f obtained by the described method are given in Table 7.

According to CEB-FIP (1991) the specific fracture energy may also be estimated by

$$G_f = G_{Fo} \, (f_{cm}/f_{cmo})^{0.7} \tag{6}$$

with f_{cmo}=10 N/mm^2 and G_{Fo} denoting the base value of the specific fracture energy depending on the maximum aggregate size $d_{\max}$. For $d_{\max}$=8 mm a base value G_{Fo}=0.025 N/mm^2 is given in CEB-FIP (1991).

4. Results

The experimental results consist of
(i) load-crack mouth opening displacement diagrams,
(ii) strain-crack mouth opening displacement diagrams and
(iii) plots of the crack-surfaces.

All data obtained from the measuring devices are corrected for possible non-linearities at low loads, which may arise from incomplete contact between the load-application roller and the specimen at the beginning of a test. Then the corrected data are smoothed by a cubic spline algorithm. All specimens show very well comparable results, which allow for the averaging of the experimental data. Thus, all diagrams in this work depict averaged curves.

One of the five specimens failed at an early stage of the experiment far before reaching the peak-load observed for the remainder of the specimens showing abnormal behavior right from the beginning of the test. Hence, this specimen was excluded from the averaging of the experimental results.

4.1. Crack mouth opening in terms of the applied load

The load in terms of the crack mouth opening displacement (CMOD) is depicted in Fig. 4. The mean-value of the peak-loads is approximately 28.0 kN. Apart from the peak-load of test PCT-3D/1 the load displacement diagrams of the four tests show good correspondence. Even the softening

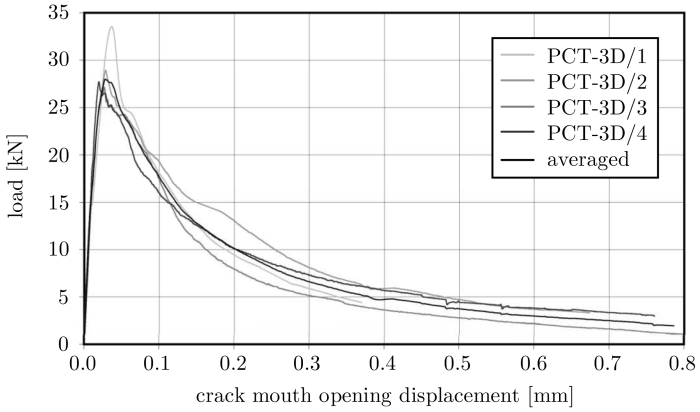

Fig. 4 Averaged load-crack mouth opening diagram from four tests on identical specimens

branches of the load-cmod diagrams of the four different tests are nearly identical.

Although the vertical displacement at the point of load-application of each specimen is measured and compensated for the vertical displacements of the supports by means of IDTs (cf. Fig. 3), the respective load-displacement curves from the different tests are characterized by a relatively large scatter and are not shown here. The scatter of these results may be explained by inaccuracies encountered when measuring near the point of load application, where local non-linearities due to the applied concentrated load may be present.

4.2. Strains at selected points in terms of the crack mouth opening

The strains measured by the six strain-gauges are documented in Figs. 5 and 6, where the strains are plotted in terms of the crack mouth opening displacement (cmod) and in terms of the applied load, respectively.

The strain-gauge SG 1, which is applied close to the notch-tip on the top face of the specimen, shows rapidly increasing strains with respect to the crack mouth opening displacement up to a value of about 103 μm/m (Fig. 5a), corresponding to a load-value of app. 23 kN (Fig. 6a). At this stage of the experiment the trace of the crack on the top surface passes by the strain-gauge SG 1, resulting in an immediate decrease of the strain. Note that the maximum value of the strain at SG 1 is found before the overall peak-load of the specimen of 28 kN is attained. In contrast to SG 1 the neighboring SG 2, located at the top surface at the edge opposite to the notch, exhibits a somewhat less steeper increase of the strain with a maximum value of about 90 μm/m (Fig. 5b) when the peak-load of the specimen is reached (Fig. 6b). The shape of the unloading branch is comparable to the one of SG 1, which indicates that the crack does not hit the strain gauge. Comparing the characteristics of these two strain gauges confirms the three-dimensional nature of the stress-state, firstly, by differences in the maximum strains and, secondly, by the maximum strains occuring at different load levels.

SG 3, located at mid-span and mid-height of the front-face, shows a maximum strain of app. 42 μm/m (Fig. 5c) at a crack mouth opening displacement of app. 0.04 mm. Hence, the peak-strain is reached at nearly the same crack mouth opening displacement as for SG 2, indicating that the crack has just separated the complete top-face and has reached the mid-height level on the front-face at

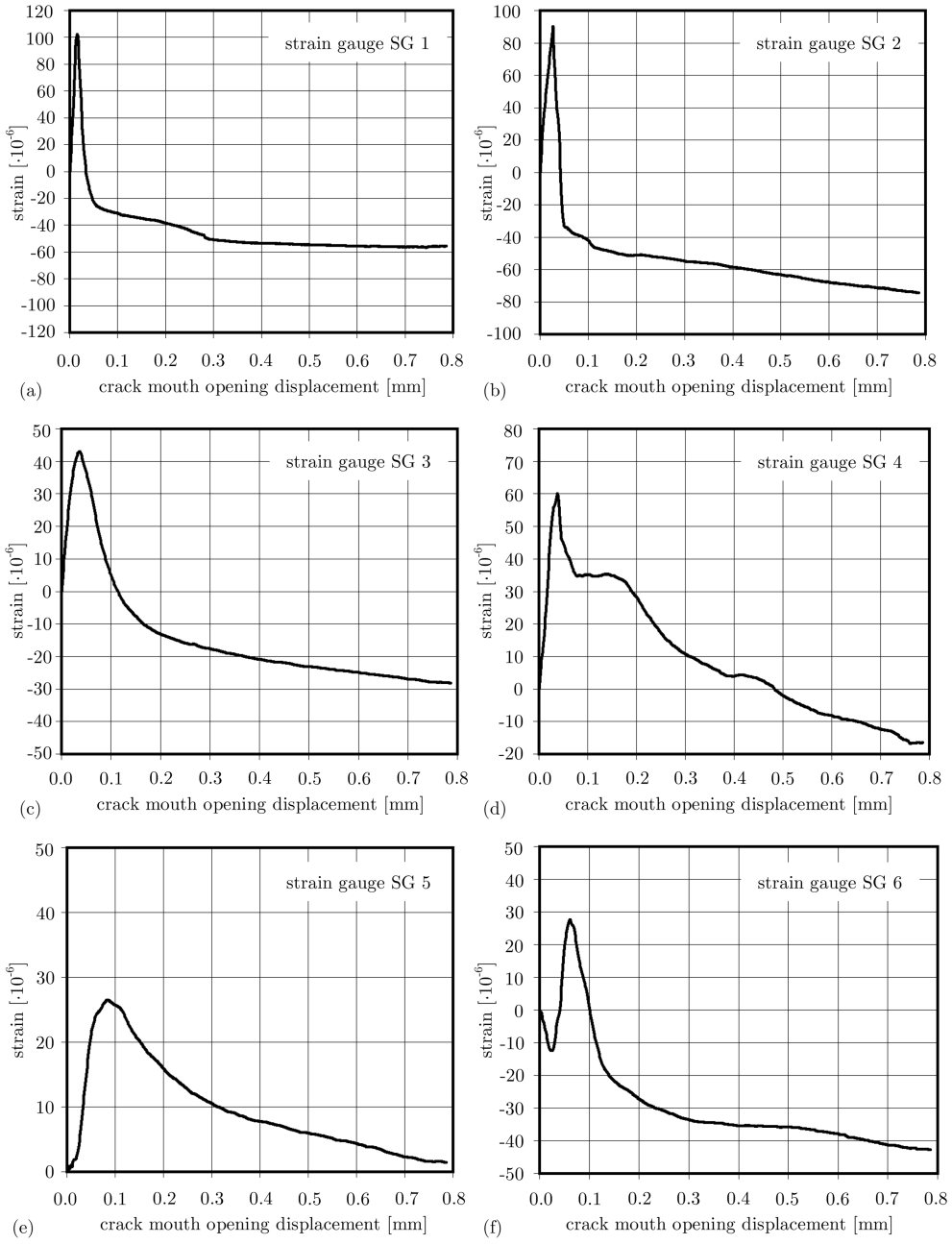

Fig. 5 Averaged strain-crack mouth opening diagrams from four tests on identical specimens

the same time. This stage in the evolution of the crack-surface corresponds to the peak-load of the specimen. SG 5, corresponding to SG 3 on the rear face, obviously shows a lower peak-strain of app. 27 μm/m (Fig. 5e) at a crack mouth opening displacement of app. 0.09 mm. This is evidently at a later stage than for SG 3 (with respect to the crack mouth opening displacement) illustrating that the crack-traces on both lateral faces are not equally propagating. Once again this demonstrates

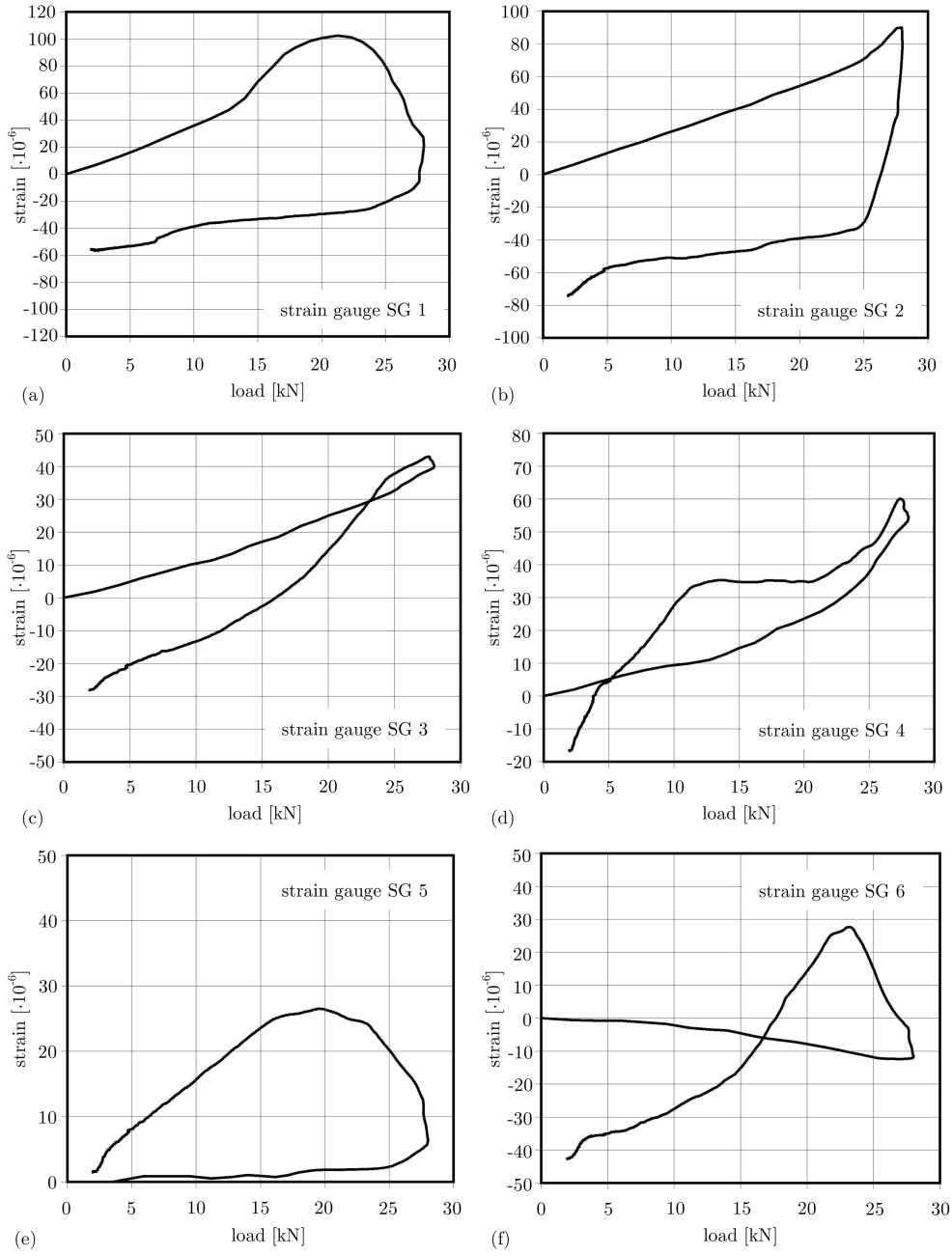

Fig. 6 Averaged strain-load diagrams from four tests on identical specimens

the three-dimensional character of the described tests.

For strain-gauge SG 4, located at mid-height of the cross-section of the load-application point on the front face, the maximum strain is app. 60 μm/m (Fig. 5d) at a crack mouth opening displacement of app. 0.04 mm. The maximum strain occurs at the same crack mouth opening displacement as the one of SG 3. As both strain gauges show an unloading branch, the crack

obviously passes between their positions. With the corresponding strain gauge SG 6 on the rear face compressive strains are measured at the first stage of loading up to the point where SG 2 reaches its peak-value and the top-surface is completely crossed by the crack (Fig. 5f). Load redistribution due to the propagating crack leads to a sign reversal of the strain rate for SG 6. When SG 3 and SG 4 attain their maximum values (corresponding to a completely cracked upper half of the front-face), SG 6 is in a strain-free state. The maximum tensile strain of app. 28 μm/m is found at almost the same crack mouth opening displacement as for SG 5, when the crack on the rear face has reached the mid-height level. From this point unloading takes place.

4.3. Crack surface

For the documentation of the crack-faces two different approaches are applied: In a first step the

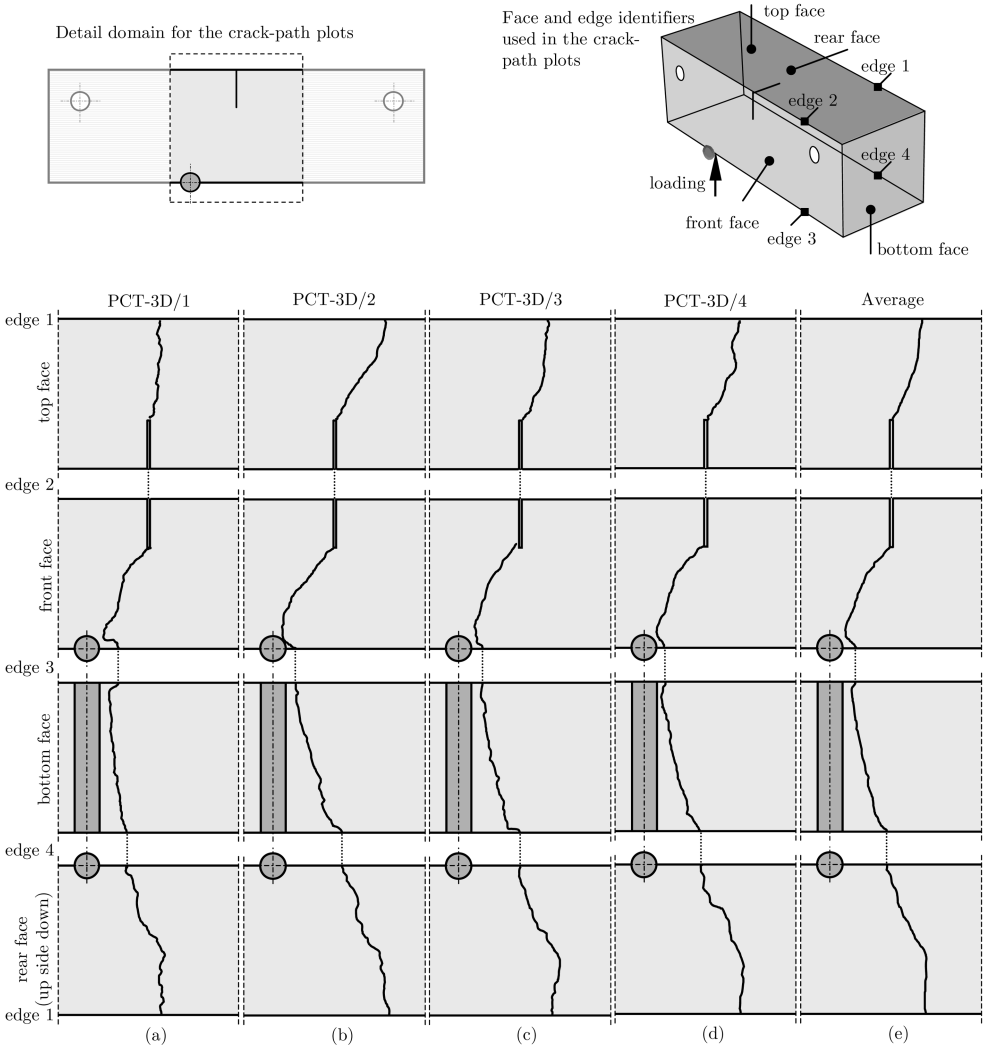

Fig. 7 (a)-(d): Crack-traces for each of the four specimens and (e) averaged crack-traces from the four tests

trace of the crack-surface on each of the four faces of a specimen is digitized. To this end, for each specimen the crack-traces are transferred onto transparencies and scanned. By means of a MATLAB based image processing tool coordinative representations of the crack-traces are extracted from which averaged crack-traces can be computed. The latter can be seen in Figs. 7(a)-(d) together with the averaged crack-traces in Fig. 7(e). It can be seen that the eccentric loading together with the eccentric notch lead to a three-dimensional, i.e., doubly curved, crack surface: The projections of

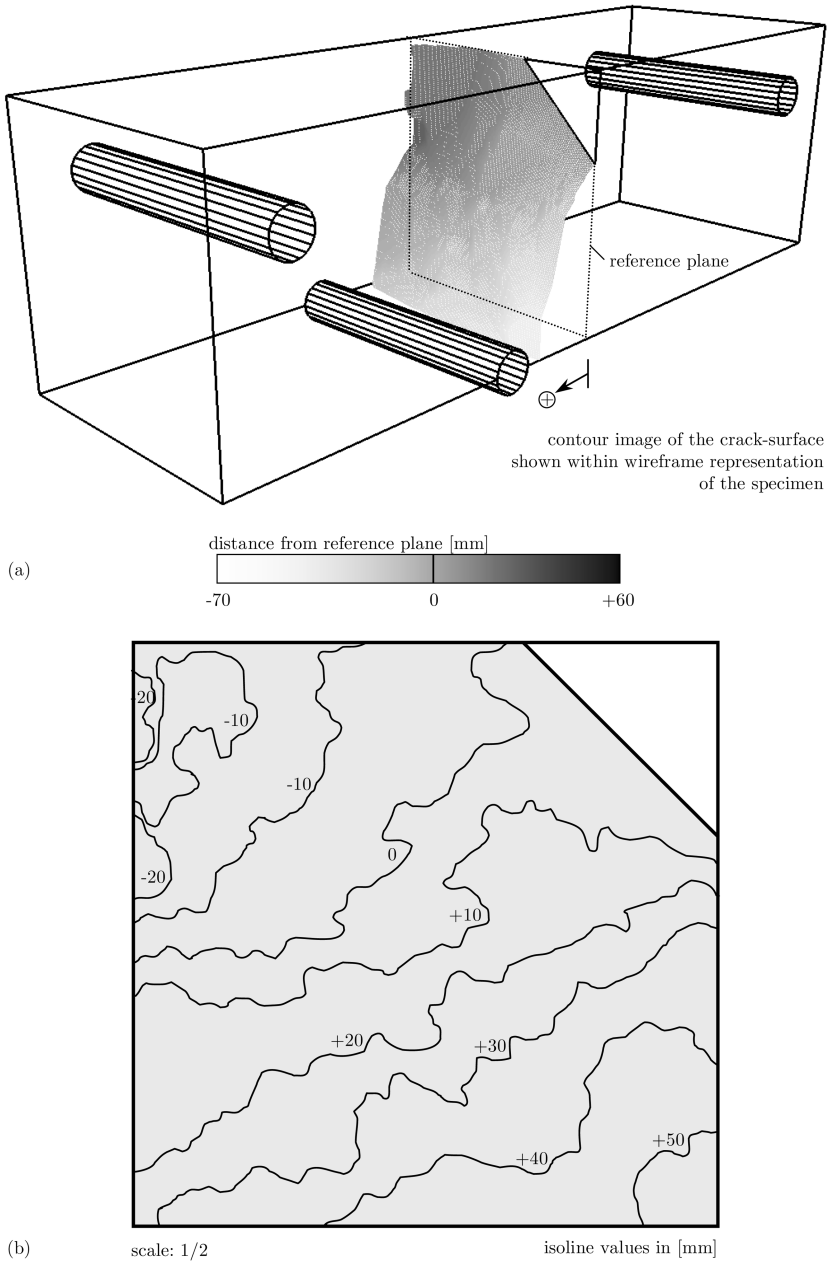

Fig. 8 Crack-surface for the first test specimen: (a) contour plot-representation and (b) isoline-representation

the crack-surface onto the top-face and the bottom-face of the specimen show considerable obliqueness and curvature. The crack-trace on the front face obviously tends towards the point of load-application, while the trace on the rear face reveals a considerable offset in the longitudinal direction.

In addition, contour-representations of the crack-surfaces for all specimens are provided in Figs. 8(a), 9(a), 10(a) and 11(a). In these figures the contour levels represent the distance of a particular point on the crack-surface from the reference-plane. The plane normal to the beam-axis at mid-span

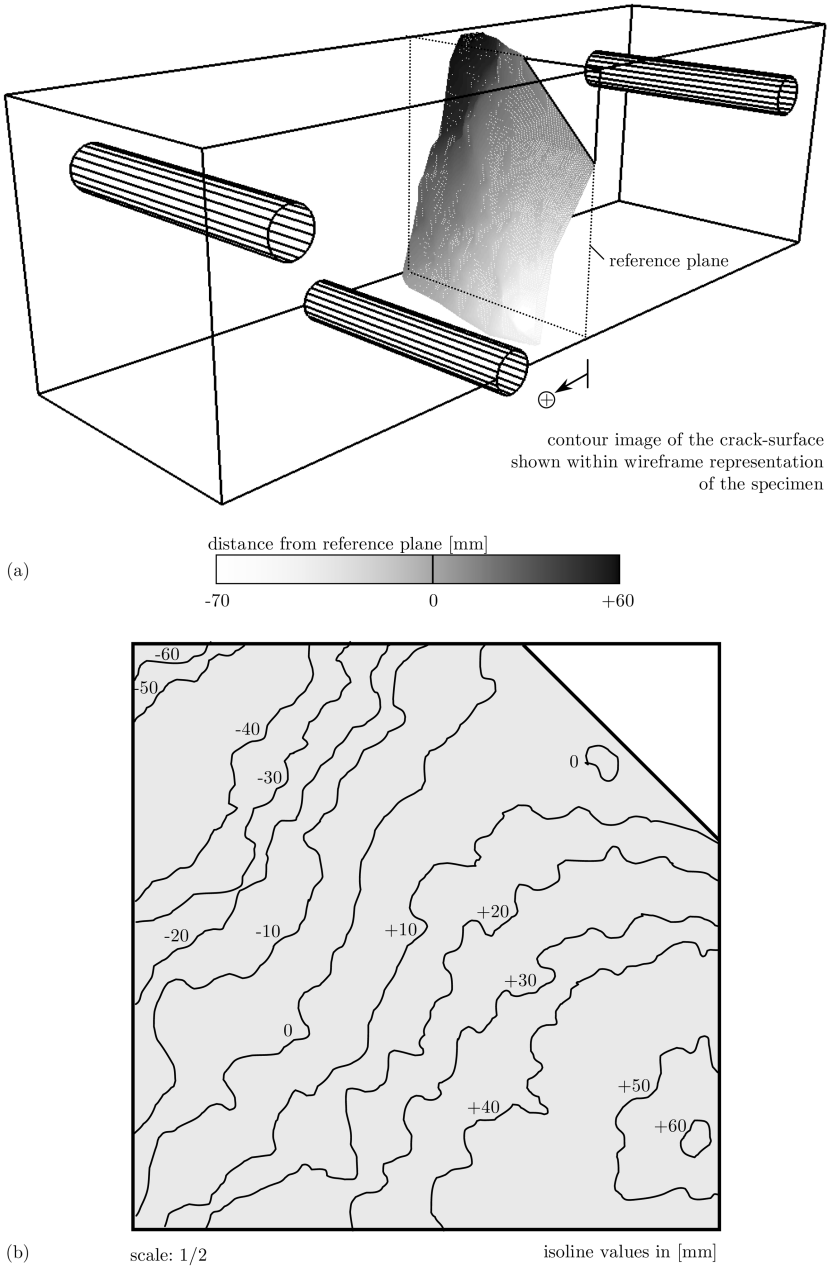

Fig. 9 Crack-surface for the second test specimen: (a) contour plot-representation and (b) isoline-representation

of the beam (i.e. the cross-section containing the notch) is chosen as the reference-plane. Isoline-representations of the respective crack-surfaces are shown in Figs. 8(b), 9(b), 10(b) and 11(b). The isolines are plotted for intervals of 10 mm; the given values are referred to the same mid-span plane as for the contour-images.

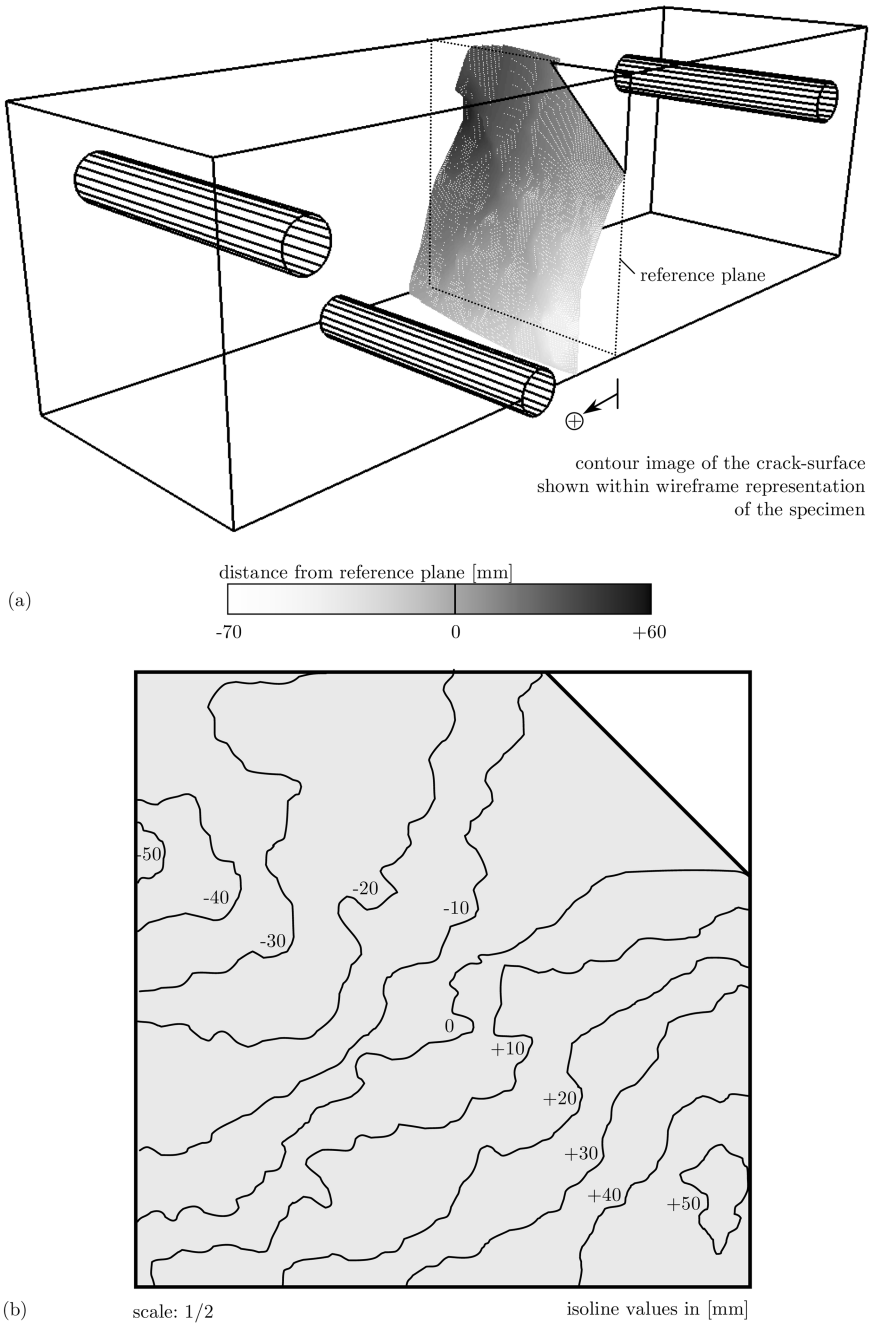

Fig. 10 Crack-surface for the third test specimen: (a) contour plot-representation and (b) isoline-representation

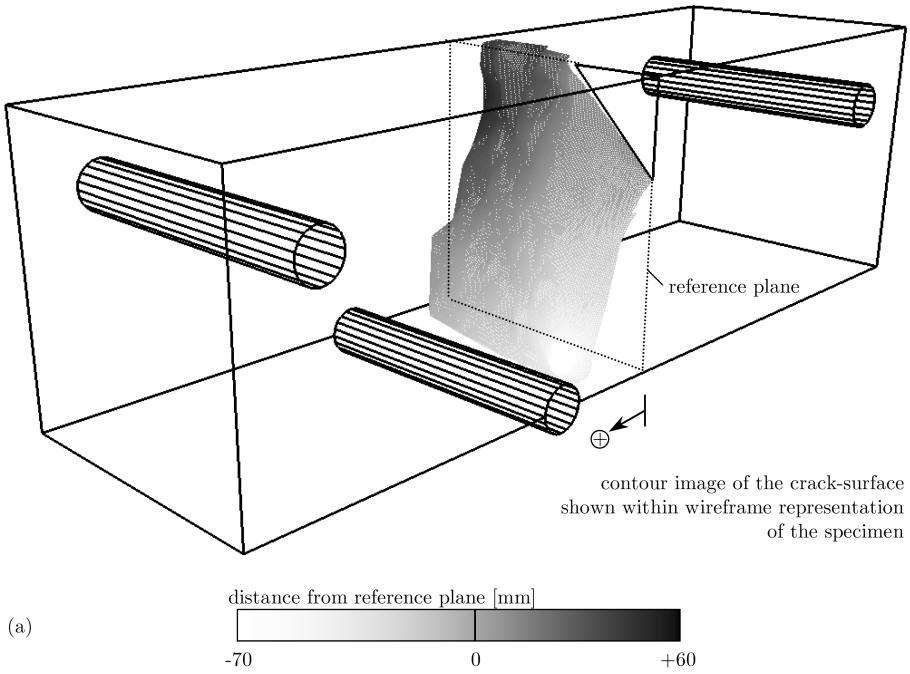

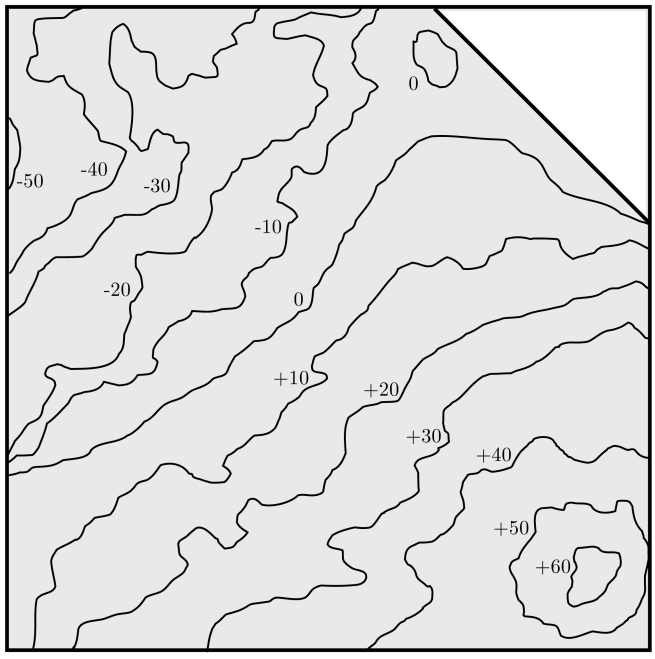

Fig. 11 Crack-surface for the fourth test specimen: (a) contour plot-representation and (b) isoline-representation

5. Summary and conclusions

In this paper a test for the validation of numerical models for cracking of plain concrete, subjected to three-dimensional stress states, was presented. The specimens were beams with an eccentric notch, which were subjected to combined bending and torsional loading, leading to the formation of a spatially curved crack-surface. The experimental results consisted of (i) load-crack mouth opening displacement diagrams, (ii) strain-crack mouth opening displacement diagrams and (iii) plots of the crack-surfaces. Four of the five tests on identical specimens showed very well comparable results, allowing the presentation of the experimental results in the form of averaged diagrams from the four tests.

References

RILEM 50-FMC (1985), "Determination of the fracture energy of mortar and concrete by means of three-point bend tests on notched beams", *RILEM, Mater. Struct.*, **18**, 285-290.

Hillerborg, A. (1985), "The theoretical basis of a method to determine the fracture energy G_F of concrete", *RILEM Mater. Struct.*, **18**, 291-296.

ENV-2006 (1990), ENV 2006 Concrete-performance, production, placing and compliance criteria.

CEB-FIP (1991), Model Code 1990, Bulletin d'information, Comité Euro-International du Béton (CEB), Laussanne.

König, G., and Grimm, R. (1996), Hochleistungsbeton, Betonkalender, Ernst & Sohn Verlag, Berlin.

Brokenshire, D.R. (1996), "A study on torsion fracture tests", Ph.D. thesis, Cardiff University.

FIP (1999), Structural Concrete - Textbook on Behaviour, Design and Performance, Fédération Internationale du Béton (FIP), Laussanne.

Jirásek, M. (2000), "Comparative study on finite elements with embedded discontinuities", *Comput. Methods Appl. Mech. Eng.*, **188**(1-3), 307-330.

Sukumar, N., Moës, N., Moran, B., and Belytschko, T. (2000), "Extended finite element method for three-dimensional crack modelling", *Int. J. Numer. Methods Eng.*, **48**, 1549-1570.

Instron, http://www.instron.com, 2002.

Matlab, http://www.mathworks.com, 2002.

Oliver, J., Huespe, A.E., and Samaniego, E. (2003), "A study on finite elements for capturing strong discontinuities", *Int. J. Numer. Methods Eng.*, **56**(14), 2135-2161.

Gasser, T.C. and Holzapfel, G.A. (2005), "Modeling 3D crack propagation in unreinforced concrete using PUFEM", *Comput. Methods Appl. Mech. Eng.*, **194**, 2859-2896.

Jefferson, A.D., Barr, B.I.G., Bennett, T., and Hee, S.C. (2004), "Three dimensional finite element simulations of fracture tests using the Craft concrete model", *Comput. Concrete*, **1**, 261-284.

Jefferson, A.D., and Bennett, T. (2005), "Benchmark problems for assessing a combined micro-mechanical continuum based model for concrete", *Proceedings of the Eighth International Conference on Computational Plasticity*, CIMNE, *Barcelona*, 197-200.

NB